Exploring the Chemical Structures and Phototochemical Properties of Graphene Oxide Derivatives by Laser Desorption/Ionization Time-of-Flight Mass Spectrometry to Develop an Efficient Platform for Mass Spectrometric Analysis

Seung-Woo Kim, Joon Young Cho, Kyoung Bin Min, Sang-Ryong Lee, Joong Tark Han,* and Young-Kwan Kim*

Read Online

ACCESS | Metrics & More | Article Recommendations | Supporting Information

ABSTRACT: Laser desorption/ionization time-of-flight mass spectrometry (LDI-TOF-MS) analysis is harnessed to investigate the chemical structure and photochemical properties of two distinct graphene oxide (GO) derivatives simultaneously. The GO derivatives are synthesized with modified Brodie's method (BGO) and Hummers' method (HGO) and characterized by LDI-TOF-MS as well as conventional tools. A series of LDI-TOF-MS analyses reveal that BGO provides higher laser energy absorption, photochemical stability, and photothermal conversion property than HGO based on their fragmentation patterns and laser desorption/ionization behavior of a thermometer molecule. Based on these characteristics, BGO exhibits higher efficiency in the LDI-TOF-MS analysis of various small molecules and synthetic polymers than HGO. These different photochemical properties of BGO are derived from its large sp^2 carbon domains compared to HGO. Based on our findings, the analytical potential of LDI-TOF-MS for GO derivatives is clearly demonstrated, which can be an efficient and unique characterization tool to explore both chemical structures and photochemical properties of various carbon materials.
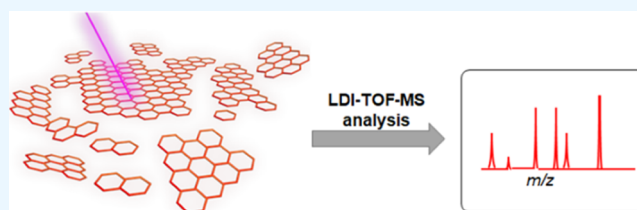
INTRODUCTION

Graphene derivatives have attracted much interest from various research fields owing to their fascinating physicochemical properties such as large surface area, high optical absorption, mechanical strength, electrical and thermal conductivity, and thermal stability.[1−3] Among them, graphene oxide (GO), an oxidized version of graphene, is one of the most important materials because of its highly tunable chemical structure and unique physicochemical properties.[3,4] These characteristics of GO originate from its special chemical structure composed of small segregated sp^2 carbon domains surrounded by the sp^3 carbon matrix presenting various oxygen functional groups. Therefore, it is an urgent issue to develop an effective characterization tool to investigate the chemical structure and physicochemical properties of this interesting material.

Laser desorption/ionization time-of-flight mass spectrometry (LDI-TOF-MS) is a promising analytical tool for GO derivatives because it provides their structural information and photochemical properties.[5,6] Our previous studies revealed the applicability of LDI-TOF-MS to explore the chemical structures, photochemical stability, and photothermal conversion property of GO derivatives based on their fragmentation patterns and laser desorption/ionization behavior of a model compound.[7,8] For instance, the lateral

dimension of GO derivatives is closely related to their degree of fragmentation during the LDI-TOF-MS analysis; large GO (LGO) sheets are more severely fragmented than small GO (SGO) sheets because LGO contains abundant labile epoxy groups on its basal plane compared to SGO.[7] The oxidative surface debris, formed during the harsh oxidation process, significantly deteriorates their laser desorption/ionization efficiency of BP on GO derivatives by interfering with laser energy absorption and subsequent transfer of the converted thermal energy from the laser absorption.[8]

However, the strong potential of LDI-TOF-MS analysis to characterize GO derivatives has not been fully demonstrated as there was no appropriate control group that exhibits distinct chemical structures and photochemical properties. In addition, the application of GO derivatives to LDI-TOF-MS analysis has been restricted to GO synthesized by Hummers' method (HGO), the most representative synthetic process of GO.[9] The basal plane of HGO is severely oxidized and thus
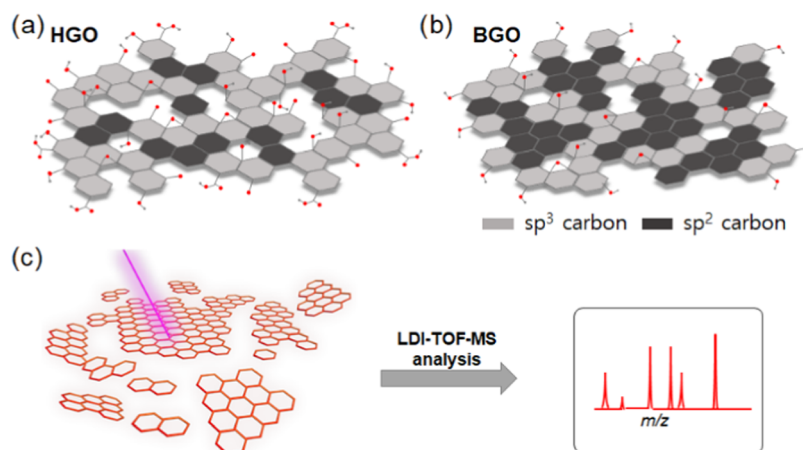
Figure 1. Schematic diagram of different structures of (a) HGO and (b) BGO, and (c) analyses of their LDI-TOF-MS behavior.

composed of numerous defects, resulting in a highly segregated structure of small sp^2 carbon domains (Figure 1a).[10,11] These structural features of HGO render it challenging to largely extend its sp^2 carbon domains for investigating the size effect of sp^2 carbon domains on the photochemical properties of GO derivatives. Therefore, the previous studies cannot provide decisive evidence but only limited information, which suggests that an appropriate model is required to fully demonstrate the potential of GO derivatives for LDI-TOF-MS application. In this regard, we recently reported that GO synthesized by modified Brodie's method (BGO) is highly aqueous-dispersible and composed of large sp^2 carbon domains compared to HGO (Figure 1b).[12] The large sp^2 carbon domains of BGO lead to its high optical absorption in the UV region, thermal stability, and recovery of electrical conductivity by the chemical reduction processes.[13] Based on the unique chemical structures and physicochemical properties of BGO, we hypothesized that it can be an excellent model contrasted with HGO to present the strong potential of LDI-TOF-MS as a distinct analytical tool for simultaneous investigation of the chemical structures and photochemical properties of GO derivatives.

Herein, BGO was synthesized by our improved protocol for eco-friendly synthesis accompanied by enhanced laser energy absorption, thermal stability, and photothermal conversion property compared to HGO. As a control, HGO was synthesized using a general protocol. The synthesized BGO and HGO were systematically characterized by conventional analytical tools to reveal differences in their chemical structures and physicochemical properties. Then, they were applied to the LDI-TOF-MS analysis to simultaneously explore their chemical structures and photochemical and photothermal properties by their fragmentation patterns and influences on the laser desorption/ionization behavior of a thermometer molecule, respectively. A series of their LDI-TOF-MS analyses clearly exhibited that BGO possesses high laser absorption capacity, photochemical stability, and photothermal conversion efficiency compared to HGO. Owing to these characteristics, BGO exhibited a higher efficiency in the LDI-TOF-MS analysis of various small molecules and synthetic polymers than HGO. Based on these findings, we confirmed that LDI-TOF-MS is a unique and powerful characterization tool for GO derivatives and think that it can be further extended to other materials.

■ EXPERIMENTAL SECTION

Chemicals and Materials. Pure graphite powder (99.999%, <200 mesh), glucose, mannitol, sucrose, His, Phe, glutathione, polyethylene glycol (PEG), and polypropylene glycol (PPG) were purchased from Alfa Aesar (Ward Hill, MA). Fuming HNO_3, sulfuric acid (98 wt %), $NaClO_3$, $KMnO_4$, HCl (37%), and H_2O_2 were purchased from Sigma-Aldrich (St. Louis, MO). Tetrahydrofuran (THF) was purchased from Daejung Chemicals (Siheung-si, Korea). Benzylpyridinium salt (BP) was synthesized by the previously reported method and used as a model compound to investigate the laser desorption process on GO derivatives through photothermal conversion.[7]

Synthesis of HGO and BGO. Graphite oxide (GpO) was synthesized using modified Brodie's and Hummers' methods.[12] To fabricate Brodie's GpO (B-GpO) powder, graphite (10 g) and $NaClO_3$ (75 g) were dry-mixed with a blade mixer. Then, fuming HNO_3 (100 mL) was added carefully into the mixed powder while kneading, and the mixture was rested for 1 h at 24 °C. After resting, massive deionized water was added to quench the oxidation reaction, and HCl (2 L) and H_2O_2 (1 L) were subsequently used to remove residual metal ions and terminate the reaction, which was by centrifugation at 10 000 rpm for 30 min at 24 °C. Finally, B-GpO powder was obtained by washing with DI water and freeze-drying. To fabricate Hummers' GpO (H-GpO) powder, graphite (5 g) was mixed with H_2SO_4 (345 mL) for 30 min, and $KMnO_4$ (15 g) was slowly added to the mixed solution with stirring. After the mixture was stirred for 72 h at 35 °C, excess deionized water was added dropwise, and the mixture was treated with H_2O_2 (0.5 L) and HCl (1 L), subsequently. The resulting solution was washed with DI water, and the precipitate was freeze-dried. The synthesized B-GpO and H-GpO powders were immersed in an ammonia solution (pH = 11) and DI water, respectively, and exfoliated using a high-speed homogenizer at 10 000 rpm for 1 h, as previously reported.[13]

Characterization. UV−vis spectra were obtained using a Cary 50 UV−vis spectrophotometer (Varian, Australia). Fourier transform infrared (FT-IR) spectra were recorded using an FT-IR-7600 (Lambda Scientific, Australia). Analytical samples of HGO and BGO were prepared using a standard KBr pellet method. Raman spectroscopic analysis of HGO and BGO was performed using an XperRam S (Nanobase, Korea). FE-SEM images of the GO sheets were obtained using an
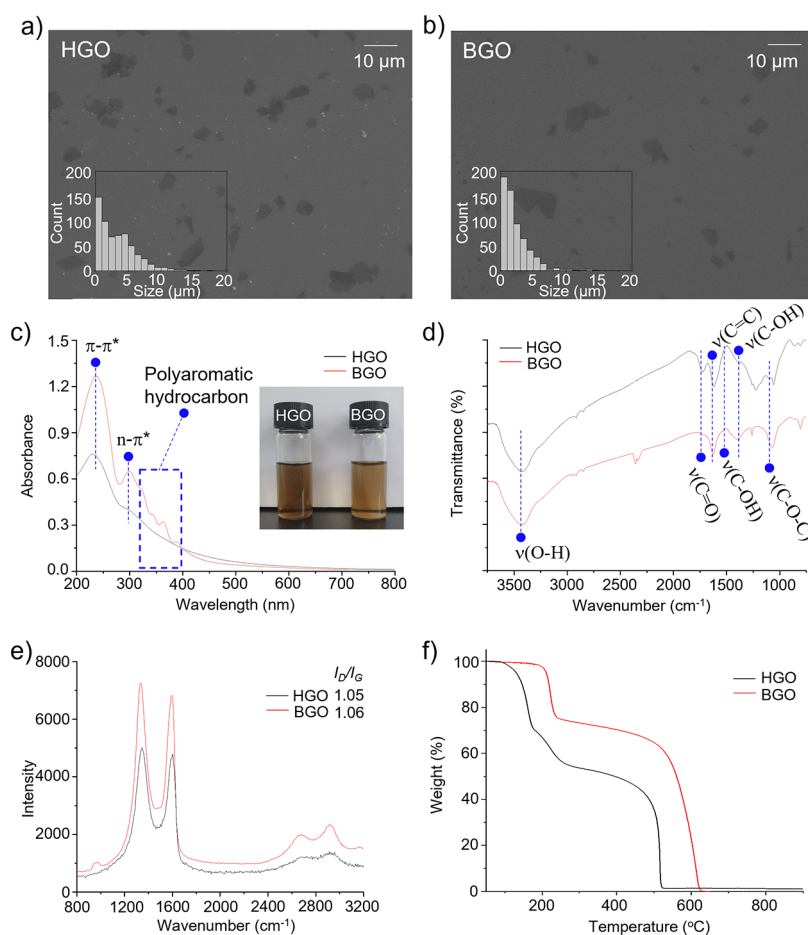
Figure 2. (a) SEM images of HGO and (b) BGO. (c) UV−vis, (d) FT-IR, (e) Raman spectra, and (f) TGA curves of HGO and BGO. The concentration of HGO and BGO suspensions was 0.1 mg mL^{-1}.

S4800 (HITACHI, Japan). Thermogravimetric analysis (TGA) of GpO was carried out using a TGA Q500 (TA instruments) in air at a ramping rate of 2 °C min^{-1}. X-ray photoelectron spectroscopy (XPS) was performed using a K-α+ system with monochromated Al Kα X-ray radiation (Thermo Fisher Scientific, U.K.). The in-plane thermal conductivity of HGO and BGO films was measured by obtaining thermal diffusivity (α) using a laser flash apparatus (LFA 467 nanoflash, NETZSCH, Germany). The thermal conductivity was calculated by the following equation: thermal conductivity = $\alpha \times \rho \times C_p$, where C_p is the specific heat capacity obtained by the laser flash method, and ρ is the density of HGO and BGO films. The thicknesses of HGO and BGO films were measured using a digimatic indicator (ID-H0530, Mitutoyo).

LDI-TOF-MS Analysis. LDI-TOF-MS analyses were carried out using IDSys (ASTA, Korea) with a 343 nm Nb:YAG laser with a pulse rate of 1 kHz and 50 μm in spot diameter at a target plate. The accelerating voltages were 18 and −18 kV in positive and negative ionization modes, respectively. All mass spectra were obtained by averaging 100 laser shots. For LDI-TOF-MS analysis, 1 μL of aqueous suspensions of BGO and HGO (0.1 mg mL^{-1}) were spotted on a stainless steel target plate. After drying under ambient conditions, the target plate was subjected to LDI-TOF-MS analysis in positive ionization mode. For LDI-TOF-MS analysis of a thermometer and small molecules, 1 μL of aqueous suspensions of BGO and HGO were spotted on the

target plate, immediately mixed by pipetting with 1 μL of methanolic solution of BP or aqueous solutions of small molecules on the target plate, and dried under ambient conditions. The target plate with the prepared spots was subjected to LDI-TOF-MS analysis in positive ionization mode with varying laser fluences.

◼ RESULTS AND DISCUSSION

BGO and HGO were synthesized using our recent protocol and Hummers' method, respectively, and systematically characterized with conventional analytical tools.[8,12] The lateral sizes of the BGO and HGO sheets were in a similar range of 1−10 μm, but the population of small-sized sheets (<3 μm) was relatively higher in BGO sheets than that in HGO sheets (Figure 2a,b). Their optical and chemical properties were analyzed with UV−vis, FT-IR, and Raman spectroscopies. UV−vis spectrum of HGO exhibited a π−π* transition band of aromatic C=C bonds at 230 nm with a shoulder from the n−π* transition of C−O bonds at approximately 300 nm (Figure 2c). In stark contrast, the UV−vis spectrum of BGO presented several distinct features from HGO. First, the π−π* transition band of BGO was observed at 237 nm, which is red-shifted compared to that of HGO (230 nm). This red shift suggests that BGO has more extended sp^2 carbon domains than HGO.[14] Second, despite their equal concentration, the absorbance from the π−π* transition band was much higher in BGO than that in HGO, which indicates that BGO has more preserved sp^2 carbon domains than HGO. Third, strong
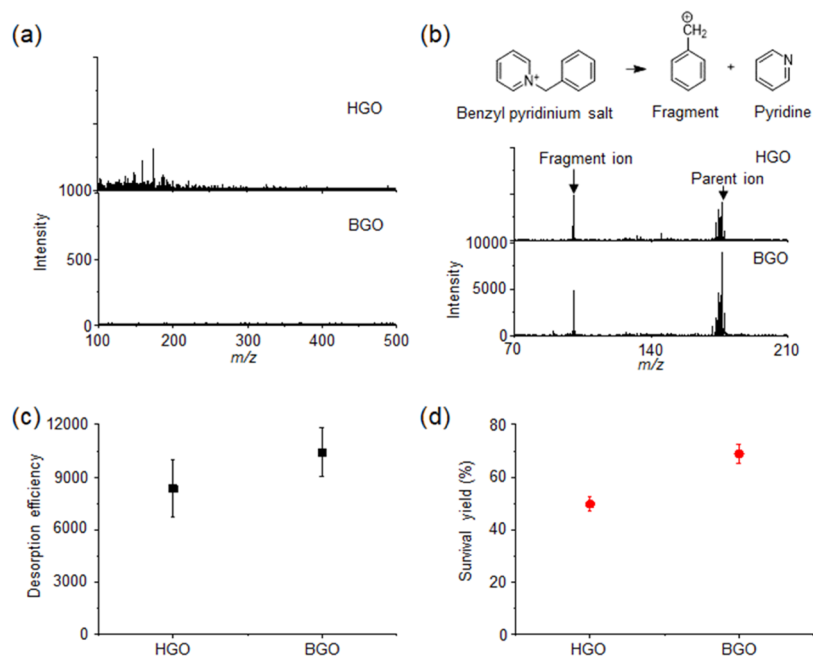
Figure 3. (a) LDI-TOF-MS spectra of HGO and BGO. (b) Fragmentation reaction of BP during LDI-TOF-MS analysis and its LDI-TOF-MS spectra obtained with BGO and HGO. (c) Desorption efficiency and (d) survival yield values of BP obtained by HGO and BGO under positive ionization modes with 16.50 mJ cm^{-2} laser fluence.

absorption bands of typical polycyclic aromatic hydrocarbon structures ranging from 300 to 350 nm were only observed in BGO, which also implies that BGO has highly extended sp^2 carbon domains compared to HGO. This spectral property is highly distinct from that of rGO derivatives, considering that the reduction processes of GO generally resulted in the red shift of the $\pi-\pi^*$ transition band and enhanced absorption in the visible region.[15] This suggests that the reduction in GO derivatives cannot lead to the formation of such a polyaromatic hydrocarbon structure in their basal plane. UV–vis spectra of HGO and BGO clearly indicate that BGO has more extended sp^2 carbon domains than HGO, although both of them were prepared by the harsh oxidation and exfoliation processes. It is also noteworthy that the absorption wavelengths of poly-aromatic hydrocarbon structures are matched with the wavelength of the laser (343 nm) used in the mass spectrometer; this optical property of BGO can greatly improve the laser absorption efficiency compared to HGO.

The FT-IR spectrum of HGO exhibited characteristic peaks derived from O−H stretching at 3430 cm^{-1}, C═O stretching at 1727 cm^{-1}, aromatic C═C stretching at 1623 cm^{-1}, O−H deformation at 1384 cm^{-1}, C−OH stretching at 1234 cm^{-1}, and C−O−C stretching at 1058 and 804 cm^{-1} (Figure 2d).[15] Compared to HGO, BGO exhibited a much weaker peak from C═O stretching but strong peaks from aromatic C═C stretching, O−H stretching, and deformation (Figure 2d). This difference in FT-IR spectra also supports that BGO has a less-oxidized structure than HGO. The C 1s XPS spectrum of HGO showed typical peaks at 284.4, 285.1, 286.5, 287.8, and 289.6 eV from sp^2 carbon (27.4%), sp^3 carbon (14.2%), C−O (43.5%), C═O (11.4%), and O−C═O (3.7%) bonds, respectively (Figure S1a). BGO also presented typical peaks at equal positions, but the composition of sp^2 carbon (37.7%), sp^3 carbon (14.7%), C−O (40.5%), C═O (4.6%), and O−C═O (2.5%) bonds was highly distinct from HGO (Figure S1b). These results clearly demonstrated that BGO has higher

sp^2 carbon content than HGO. In spite of the less-oxidized structure, the aqueous dispersibility of BGO was comparable to that of HGO (Figure 2c).[11] For further evaluation of the structure of HGO and BGO, Raman spectroscopic analysis was carried out, and there were typical D and G peaks originating from their defective and ordered sp^2 carbon domains, respectively. The D and G peaks of BGO were observed at 1345 and 1601 cm^{-1}, respectively, but these peaks were slightly downshifted to 1325 and 1588 cm^{-1} from HGO, which indicates the different distribution of defects on their basal plane (Figure 2e).[16] It is worth noting that the D peak of HGO was broad compared to that of BGO, implying that HGO has a more defective structure than BGO.[17] The intensity ratio of 2D and G peaks (I_{2D}/I_G) was also higher in BGO (0.29) than that in HGO (0.25), and this result indicated that HGO is composed of a more graphene-like structure than HGO (Figure 2e).[18] TGA was performed to determine the thermal stabilities of HGO and BGO. The weight loss of HGO started at 95 °C with an inflection point at 257 °C from the gasification of oxygen functional groups. The major weight loss occurred at approximately 450 °C from the thermal degradation of the sp^2 carbon framework (Figure 2f). The TGA curve of BGO is distinct from that of HGO. The first weight loss started at 180 °C without an inflection point, and the major weight loss point was also at approximately 500 °C (Figure 2f). The high thermal decomposition temperatures of BGO show that it is thermally stable compared to HGO. These spectral and thermal degradation features match well with our previous results, indicating that BGO is composed of fewer defects in their basal plane than HGO.[13]

LDI-TOF-MS analysis of HGO and BGO was carried out to reveal the correlation between their chemical structure and fragmentation behavior under the equal condition of laser irradiation under high vacuum. The LDI-TOF-MS spectrum of HGO presented many unassignable peaks in the low-mass region (<200 m/z) with broad background noise (Figure 3a).

In stark contrast, there was no background signal from BGO (Figure 3a). Similar fragmentation behavior was also observed in negative ionization mode (Figure S2). Based on our previous report, the degree of fragmentation during LDI-TOF-MS analysis is closely related to the chemical and physical structures of GO derivatives.[7] LGO sheets presented higher fragmentation than SGO sheets because the basal plane of LGO sheets is composed of many labile functional groups compared to that of SGO sheets. In this regard, the relieved fragmentation behavior implies that BGO sheets are more stable under the laser irradiation during LDI-TOF-MS analysis than HGO sheets, and this higher stability concurred well with their well-preserved sp^2 carbon network as shown by their UV−vis and Raman spectra. (Figure 2c,e) It is also noteworthy that BGO exhibited higher laser energy absorption (343 nm) than HGO, owing to its highly preserved sp^2 carbon structure, and thus, the surface temperature of BGO might be more rapidly and highly elevated than that of HGO under similar conditions. Based on these results, we find that LDI-TOF-MS analysis clearly reveals that BGO provides a distinct structure and superior photochemical stability to HGO.

The photothermal conversion properties of HGO and BGO were investigated with the LDI-TOF-MS analysis of a model thermometer molecule, BP. BP has been widely used to explore the laser desorption/ionization mechanism on the surface of nanomaterials through photothermal conversion because it has an intrinsic positive charge on its structure and thus enables to exclusively focus on its photothermal desorption as either intact or fragmented ions from the surface of nanomaterials.[19−21] The survival yield and desorption efficiency were estimated by dividing the parent ion intensity by the total ion intensity of parent and fragmented ions and by summing the absolute intensity of the parent and fragmented ions, respectively (Figure 3c,d). The average desorption efficiency values for BGO and HGO were estimated to be 10 411 ± 1385 and 8352 ± 1630, respectively (Figure 3c,d). This higher desorption efficiency value of BGO indicates that it can more efficiently convert laser energy into thermal energy than HGO during the LDI-TOF-MS analysis process, and thus, it can be derived from its efficient electron−phonon interaction resulting from the highly preserved sp^2 carbon network. Interestingly, despite the higher desorption efficiency value of BGO compared to that of HGO (Figure 3c), the average survival yield value of BGO (68.8 ± 3.5%) was also higher than that of HGO (49.7 ± 2.7%, Figure 3d). Considering that a high desorption efficiency value can be obtained by the photothermal desorption process of BP on nanomaterials, it is generally accompanied by a low survival yield value resulting from the thermal fragmentation of BP.[22] However, BGO presented higher desorption efficiency and survival yield values than HGO, implying that it provided a distinct laser desorption/ionization process for BP compared to HGO. This difference might originate from their disparate chemical structures and photothermal properties.[23] It is worth noting that the affinity of BP to BGO and HGO can also affect its laser desorption/ionization behavior because the strong affinity of BP to nanomaterials can lower its desorption efficiency and survival yield.[24] In this point of view, HGO has more negatively charged functional groups such as hydroxyl and carboxylic acid (Figures 2d and S1) and thus stronger affinity to positively charged BP than BGO, implying that this factor can contribute different laser desorption/ionization behaviors of BP on their surfaces. Despite this potential affinity

effect, we think that the distinct laser desorption/ionization behavior of BP on BGO and HGO was mainly derived from the highly preserved sp^2 carbon structure of BGO compared to HGO, resulting in high laser absorption, photothermal conversion, and thermal and photochemical stability (Figures 2c, and 3a). This structural difference between BGO and HGO might result in a sequential process including efficient laser energy absorption and photothermal conversion without structural destruction by laser irradiation during LDI-TOF-MS analysis.

To further clarify the structural uniqueness of BGO, a control experiment was performed with reduced GO (rGO) derivatives. HGO and BGO were equally treated by heating in alkaline conditions to induce their partial chemical reduction in water without using surfactants for their dispersion because these additives can be adsorbed on the surface of HGO and BGO and affect the laser desorption/ionization process on their surfaces.[8] During the chemical reduction for 90 min, the optical absorption of HGO gradually changed with a red shift of its π−π* transition band from 230 to 234 nm, decrease of the n−π* transition band, and increase of absorption in the visible region. These changes are well-matched with the previous reports and indicated that HGO was successfully reduced under experimental conditions (Figure S3a).[14] On the other hand, the π−π* transition band of BGO was not shifted, and there was only a slight increase of the n−π* transition band after 90 min of the reduction reaction (Figure S3b). These results indicated that BGO was more chemically stable than HGO in alkaline conditions and clearly showed that the unique optical absorption property of BGO, which originated from its typical polycyclic aromatic hydrocarbon structures, cannot be simply achieved by chemical reduction of HGO. The different degree of chemical reduction of HGO and BGO was further confirmed by analysis results with FT-IR (Figure S3c,d) and XPS analysis (Figure S4). Then, the fragmentation behaviors of rHGO and rBGO derivatives were examined with LDI-TOF-MS analysis under both positive and negative ionization modes. After 30 min of chemical reduction, the fragmentation of HGO was considerably alleviated under both positive and negative ionization modes at the same LDI-TOF-MS conditions (Figure S5). In the case of BGO, it was intrinsically stable without chemical reduction compared to HGO, and there was no noticeable change along with the chemical reduction (Figure S5). The laser desorption/ionization behavior of BP was also explored on the rHGO and rBGO derivatives. As shown in Figure 3, HGO and BGO initially presented distinct desorption efficiency and survival yield values, but there was no significant change in their desorption efficiency and survival yield values along with chemical reduction (Figure 4). Considering that the oxygen functional groups of HGO decreased during chemical reduction, the affinity between BP and HGO continuously decreased, but the laser desorption/ionization behavior of BP was not affected by the chemical reduction process. This result implied that the affinity of BP to HGO has negligibly influenced its laser desorption/ionization behavior. The results also confirmed that the unique photochemical properties of BGO cannot be simply reenacted by the chemical reduction of HGO.

Although the high laser desorption/ionization efficiency of BGO can be understood by its high photochemical stability and laser absorption capacity, it is still unclear that how BGO can provide higher desorption efficiency and survival yield
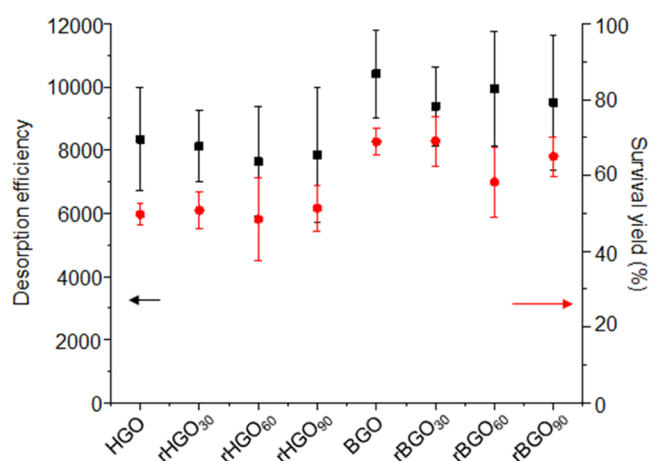
Figure 4. Desorption efficiency and survival yield values of BP obtained from HGO, BGO and their reduced derivatives prepared with different reduction times under positive ionization modes at 16.50 mJ cm^{-2} laser fluence.

values than HGO. To address this issue, the specific heat capacity and thermal conductivity of BGO and HGO were examined by using laser flash apparatus. For the measurement, the laminated films of BGO and HGO were fabricated with the vacuum-assisted filtration process to obtain macroscopically assembled materials with an analogous internal structure. The thicknesses of HGO and BGO films were respectively measured to be 182 ± 4 and 188 ± 6 μm, respectively, and the resulting films exhibited a typical laminated structure of GO derivatives (Figure S6). The specific heat capacity of BGO was 8.485 J g^{-1} K^{-1}, which was lower than that of HGO (9.616 J g^{-1} K^{-1}). In addition, the in-plane thermal conductivity of BGO films was measured to be 13.125 ± 0.612 W m^{-1} K^{-1}, and this value was also lower than that of HGO films (24.838 ± 2.763 W m^{-1} K^{-1}). The lower specific heat capacity and thermal conductivity are commonly preferable to a more efficient laser desorption/ionization process on the surface of BGO than that on the HGO surface because the surface temperature of BGO can be rapidly elevated when it was

irradiated with a laser source, and the localized heating was maintained with low thermal dissipation.[21,22]

The laser desorption/ionization behavior of BP on BGO and HGO was further explored with varying laser fluence from 1.12 to 1.34 mJ cm^{-2} for the mechanistic study of the laser desorption/ionization process. The parent and fragment ions of BP started to be detected on BGO at 1.12 mJ cm^{-2} laser fluence, and their desorption efficiency and survival yield values were calculated to be 73 ± 23 and 70 ± 2%, respectively (Figure 5a,b). By stark contrast, these ions were not detected on HGO at the same conditions and started to be detected at 1.20 mJ cm^{-2} laser fluence with the desorption efficiency and survival yield values of 709 ± 192 and 78 ± 2%, respectively (Figure 5a,b). At the same conditions, the desorption efficiency and survival yield values of BP on BGO were calculated to be 7441 ± 623 and 91 ± 1%, respectively (Figure 5a,b). BGO presented nearly 10 fold-higher desorption efficiency than HGO in spite of its higher survival yield than HGO, and this result concurred well with the LDI-TOF-MS analysis of BP at 16.50 mJ cm^{-2} laser fluence (Figures 3 and 5). It is also worth noting that although BGO is thermally exploded at 1.34 mJ cm^{-2} laser fluence, BP ions are clearly detected at 1.14 mJ cm^{-2} before its explosion, indicating that the laser desorption/ionization process on BGO mainly occurred through the thermally driven desorption process (Figure 5c).[21] On the other hand, the thermal explosion of HGO is simultaneously observed with laser desorption/ ionization of BP at 1.20 mJ cm^{-2}, implying that the laser desorption/ionization process on HGO mainly proceeded by the phase-transition-driven process (Figure 5c).[22] The strong laser absorption, high thermal stability, low specific heat capacity, and thermal conductivity of BGO can synergistically lead to rapidly reaching a high temperature under low laser fluence without its structural destruction, resulting in an efficient photothermal laser desorption/ionization process of BP. Therefore, it is reasonable to conclude that LDI-TOF-MS analysis can be an efficient and special characterization tool for exploring the structure and property correlation of GO derivatives.
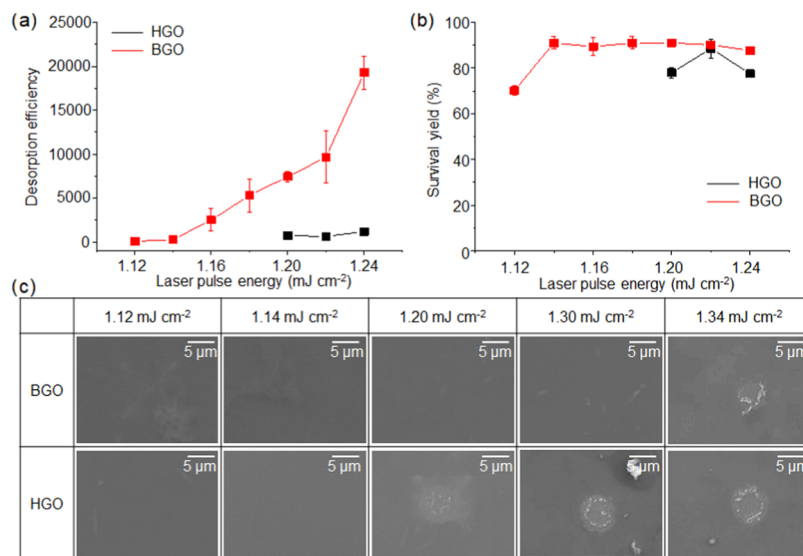

Figure 5. (a) Desorption efficiency and (b) survival yield values of BP obtained on BGO and HGO as a function of laser fluence in LDI-TOF-MS analysis. (c) SEM images of BGO and HGO layers after laser irradiation with different laser fluences.
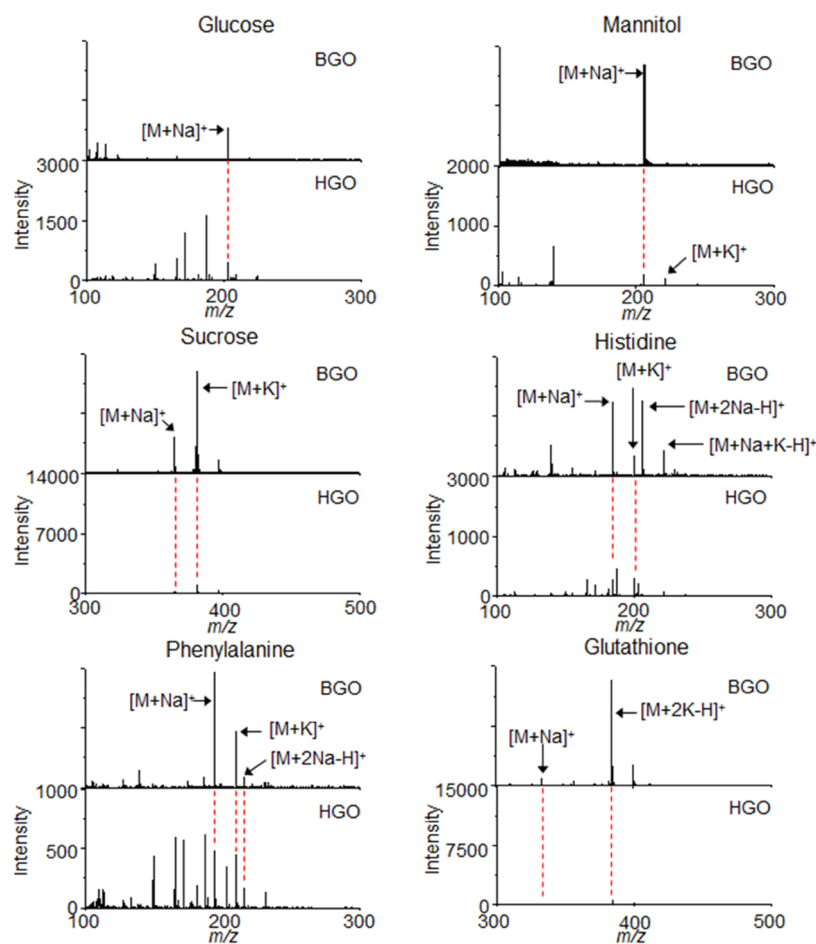
Figure 6. LDI-TOF-MS spectra of 1 nmol of glucose, mannitol, sucrose, histidine, phenylalanine, and glutathione obtained with HGO and BGO under positive ionization modes with 16.50 mJ cm^{-2} laser fluence.

Encouraged by interesting findings from LDI-TOF-MS analyses of BP, the laser desorption/ionization efficiency of HGO and BGO was explored using various small molecules, such as glucose, mannitol, sucrose, His, Phe, and glutathione dissolved in water. The small molecules (1 nmol) were subjected to LDI-TOF-MS analysis with HGO and BGO. All of the tested small molecules were successfully detected with both BGO and HGO as sodium and/or potassium adducts at m/z 203 [glucose + Na]$^+$, 205 [mannitol + Na]$^+$, 221 [mannitol + K]$^+$, 365 [sucrose + Na]$^+$, 381 [sucrose + K]$^+$, 178 [His + Na]$^+$, 194 [His + K]$^+$, 200 [His + 2Na − H]$^+$, 216 [His + Na + K − H]$^+$, 188 [Phe + Na]$^+$, 204 [Phe + K]$^+$, 210 [Phe + 2Na − H]$^+$, 330 [glutathione + Na]$^+$, and 385 [glutathione + 2 K − H]$^+$ (Figure 6). BGO exhibited high mass signal intensity with a low background signal from all tested small molecules compared to HGO. In particular, glutathione, a small peptide (exact mass: 307 Da), was detected with a high S/N ratio using BGO, but there was a negligible mass signal with HGO (Figure 6). The limit of detection (LOD) values of glucose, mannitol, sucrose, His, Phe, and glutathione were 100, 50, 25, 100, 100, and 100 pmol, respectively, with HGO (Figure S7) and 100, 10, 25, 100, 100, and 10 pmol, respectively, with BGO (Figure S8). BGO showed lower LOD values for mannitol and glutathione than HGO. In addition, there were more unassignable peaks from the mass spectra obtained with HGO than those with BGO. These results concur with their LDI-TOF-MS spectra (Figure 3a) and laser

desorption/ionization behavior of BP. Taken together, it was clearly confirmed that BGO more effectively converted laser energy into thermal energy for laser desorption/ionization of various small molecules with less background noise from fragmentation than HGO (Figure 6).

In addition to small molecules, the LDI-TOF-MS analysis of synthetic polymers, i.e., PEG and PPG with molecular weights of 1000 and 2000 Da, was also carried out to explore the effect of the different laser desorption/ionization characteristics on synthetic polymers. Interestingly, BGO presented the LDI-TOF-MS spectra of PEG$_{1000}$ and PEG$_{2000}$ with a characteristic Gaussian distribution of molecular weight (intervals of 44 Da corresponding to its repeating unit, −C$_2$O$_1$H$_4$−) centered at approximately m/z 1000 and 2000, which are in good agreement with the average molecular weights provided by the company (Figure 7a). In stark contrast, the LDI-TOF-MS spectra of PEG$_{1000}$ and PEG$_{2000}$ obtained with HGO showed no Gaussian distribution; furthermore, the majority of mass peaks were detected below an m/z of 600, implying that most of polymeric chains were fragmented during LDI-TOF-MS analysis (Figure 7a). These results are in good agreement with the higher desorption efficiency and survival yield values of BGO, indicating that BGO results in a more soft and efficient laser desorption/ionization process than HGO. To further examine this finding, PPG$_{1000}$ and PPG$_{2000}$ were also subjected to LDI-TOF-MS analysis with HGO and BGO, and analogous behaviors were observed from their LDI-TOF-MS spectra,
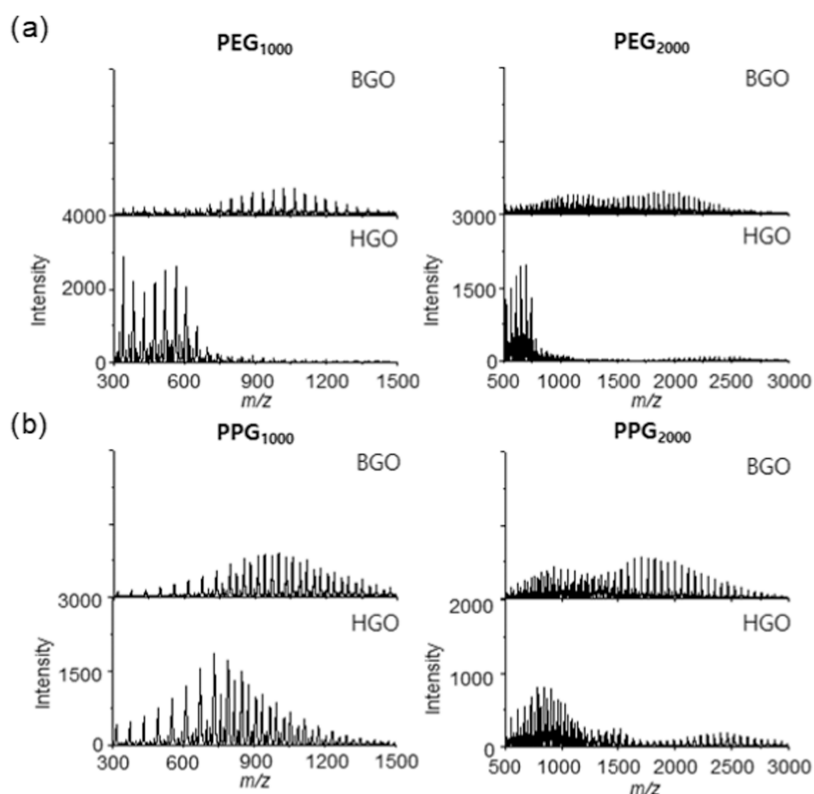
Figure 7. LDI-TOF-MS spectra of (a) PEG_{1000} and PEG_{2000} and (b) PPG_{1000}, and PPG_{2000} obtained with HGO and BGO under the positive ionization modes.

confirming that BGO provides a more soft and efficient laser desorption/ionization process than HGO (Figure 7b). Taken together, we found that BGO is a unique and efficient matrix for the LDI-TOF-MS analysis of small molecules as well as synthetic polymers because of its extended sp^2 carbon domains. In fact, this leads to high laser absorption, photochemical stability, and photothermal conversion.

CONCLUSIONS

We demonstrated the potential of LDI-TOF-MS analysis to simultaneously investigate the structure and photochemical properties of GO derivatives using HGO and BGO as a model. Despite the higher laser energy absorption of BGO compared to that of HGO, laser-induced fragmentation was greatly alleviated in BGO compared to HGO during LDI-TOF-MS analysis. In addition, higher desorption efficiency and survival yield values of BP were obtained with BGO and thus it provided better performance for the LDI-TOF-MS analysis of various small molecules and synthetic polymers. The systematic series of LDI-TOF-MS analyses revealed that BGO provides higher laser energy absorption, photochemical stability, and photothermal conversion than HGO owing to its distinct highly extended sp^2 carbon domains. It is noteworthy that the distinct chemical structure and photochemical properties of BGO cannot be achieved by simple chemical reduction of HGO. We believe that this study can provide fundamental insights and useful information to characterize both chemical structures and physicochemical properties of GO derivatives by LDI-TOF-MS.

ASSOCIATED CONTENT

Supporting Information

The Supporting Information is available free of charge at https://pubs.acs.org/doi/10.1021/acsomega.2c05464.

Experimental section for the reduction of HGO and BGO; C 1s XPS spectra and LDI-TOF-MS spectra of HGO and BGO obtained under negative ionization mode; UV−vis, FT-IR, C/O ratio, and LDI-TOF-MS spectra of reduced HGO and BGO; SEM images of HGO and BGO films; and LOD test results of small molecules on HGO and BGO (PDF)

AUTHOR INFORMATION

Corresponding Authors

Joong Tark Han − Nano Hybrid Technology Research Center, Korea Electrotechnology Research Institute (KERI), Changwon 51543, Republic of Korea; Department of Electro-Functionality Material Engineering, University of Science and Technology (UST), Changwon 51543, Republic of Korea; orcid.org/0000-0002-3351-3975; Email: jthan@keri.re.kr

Young-Kwan Kim − Department of Chemistry, Dongguk University-Seoul, Seoul 04620, South Korea; orcid.org/0000-0002-9929-9510; Email: kimyk@dongguk.edu

Authors

Seung-Woo Kim − Department of Chemistry, Dongguk University-Seoul, Seoul 04620, South Korea

Joon Young Cho − Nano Hybrid Technology Research Center, Korea Electrotechnology Research Institute (KERI), Changwon 51543, Republic of Korea; Department of Electro-

Functionality Material Engineering, University of Science and Technology (UST), Changwon 51543, Republic of Korea

Kyoung Bin Min − *Department of Chemistry, Dongguk University-Seoul, Seoul 04620, South Korea*

Sang-Ryong Lee − *Department of Biological and Environmental Science, Dongguk University-Seoul, Goyang-si, Gyeonggi-do 10326, Republic of Korea*

Complete contact information is available at:
https://pubs.acs.org/10.1021/acsomega.2c05464

Author Contributions

S.-W.K.: methodology, investigation, data curation, and writing—original draft. J.Y.C.: data curation, resource, and data curation. K.B.M.: investigation and writing—review & editing. S.-R.L.: formal analysis, resource, and funding acquisition. J.T.H.: methodology, data curation, resources, supervision, funding acquisition, and writing—original draft. Y.-K.K.: conceptualization, supervision, data curation, resources, funding acquisition, writing—original draft, and writing—review & editing.

Notes

The authors declare no competing financial interest.

■ ACKNOWLEDGMENTS

■ REFERENCES

(1) Zhao, G.; Li, X.; Huang, M.; Zhen, Z.; Zhong, Y.; Chen, Q.; Zhao, X.; He, Y.; Hu, R.; Yang, T.; Zhang, R.; Li, C.; Kong, J.; Xu, J. B.; Ruoff, R. S.; Zhu, H. The physics and chemistry of graphene-on-surfaces. *Chem. Soc. Rev.* **2017**, *46*, 4417−4449.

(2) Jo, G.; Choe, M.; Lee, S.; Park, W.; Kahng, Y. H.; Lee, Takhee. The application of graphene as electrodes in electrical and optical devices. *Nanotechnology* **2012**, *23*, No. 112001.

(3) Chung, C.; Kim, Y. −K.; Shin, D.; Ryoo, S. −R.; Hong, B. H.; Min, D. −H. Biomedical applications of graphene and graphene oxide. *Acc. Chem. Res.* **2013**, *46*, 2211−2224.

(4) Loh, K. P.; Bao, Q.; Eda, G.; Chhowalla, M. Graphene oxide as a chemically tunable platform for optical applications. *Nat. Chem.* **2010**, *2*, 1015−1024.

(5) Chu, H. W.; Mao, J. Y.; Lien, C. W.; Hsu, P. H.; Li, Y. J.; Lai, J. Y.; Chiu, T. C.; Huang, C. C. Pulse laser-induced fragmentation of carbon quantum dots: a structural analysis. *Nanoscale* **2017**, *9*, 18359−18367.

(6) Šedo, O.; Alberti, M.; Janča, J.; Havel, J. Laser desorption−ionization time of flight mass spectrometry of various carbon materials. *Carbon* **2006**, *44*, 840−847.

(7) Kim, Y. K.; Min, D. H. The structural influence of graphene oxide on its fragmentation during laser desorption/ionization mass spectrometry for efficient small-molecule analysis. *Chem. - Eur. J.* **2015**, *21*, 7217−7223.

(8) Hong, Y. L.; Lee, J.; Ku, B. C.; Kang, K.; Lee, S.; Ryu, S.; Kim, Y. K. The influence of oxidative debris on the fragmentation and laser desorption/ionization process of graphene oxide derivatives. *New J. Chem.* **2018**, *42*, 12692−12697.

(9) Hummers, W. S.; Offeman, R. E. Preparation of graphitic oxide. *J. Am. Chem. Soc.* **1958**, *80*, 1339.

(10) Erickson, K.; Erni, R.; Lee, Z.; Alem, N.; Gannett, W.; Zettl, A. Determination of the local chemical structure of graphene oxide and reduced graphene oxide. *Adv. Mater.* **2010**, *22*, 4467−4472.

(11) Cho, J. Y.; Jang, J. I.; Lee, W. K.; Jeong, S. Y.; Hwang, J. Y.; Lee, H. S.; Park, J. H.; Jeong, S. Y.; Jeong, H. J.; Lee, G. W.; Han, J. T. Fabrication of high-quality or highly porous graphene sheets from exfoliated graphene oxide via reactions in alkaline solutions. *Carbon* **2018**, *138*, 219−226.

(12) Cho, J. Y.; Kim, J. H.; Yang, H. J.; Park, J. H.; Jeong, S. Y.; Jeong, H. J.; Lee, G. W.; Han, J. T. Tailored and highly efficient oxidation of various-sized graphite by kneading for high-quality graphene nanosheets. *Carbon* **2020**, *157*, 663−669.

(13) Cho, J. Y.; Kim, J. H.; Han, J. T. Extraordinary thermal behavior of graphene oxide in air for electrode applications. *Nanoscale Adv.* **2021**, *3*, 1597.

(14) Hidayah, N. M. S.; Liu, W. W.; Lai, C. W.; Noriman, N. Z.; Khe, C. S.; Hashim, U.; Lee, H. C. Comparison on graphite, graphene oxide and reduced graphene oxide: Synthesis and characterization. *AIP Conf. Proc.* **2017**, *1892*, 15002.

(15) Jeon, J.; Choi, M.; Kim, S. B.; Seo, T. H.; Ku, B. C.; Ryu, S.; Park, J. H.; Kim, Y. K. Eggshell membrane hydrolysate as a multifunctional agent for synthesis of functionalized graphene analogue and its catalytic nanocomposites. *J. Ind. Eng. Chem.* **2021**, *102*, 233−240.

(16) Kwon, Y. −B.; Lee, S. −R.; Seo, T. H.; Kim, Y. −K. Fabrication of a strong artificial nacre based on tannic acid-functionalized graphene oxide and poly(vinyl alcohol) through their multidentate hydrogen bonding. *Macromol. Res.* **2022**, *30*, 279−284.

(17) Kaniyoor, A.; Ramaprabhu, S. A Raman spectroscopic investigation of graphite oxide derived graphene. *AIP Adv.* **2012**, *2*, No. 032183.

(18) Arul, R.; Oosterbeek, R. N.; Robertson, J.; Xu, G.; Jin, J.; Simpson, M. C. The mechanism of direct laser writing of graphene features into graphene oxide films involves photoreduction and thermally assisted structural rearrangement. *Carbon* **2016**, *99*, 423−431.

(19) Kawasaki, H.; Nakai, K.; Arakawa, R.; Athanassiou, E. K.; Grass, R. N.; Stark, W. J. Functionalized graphene-coated cobalt nanoparticles for highly efficient surface-assisted laser desorption/ionization mass spectrometry analysis. *Anal. Chem.* **2012**, *84*, 9268−9275.

(20) Hong, Y. L.; Seo, T. H.; Jang, H.; Kim, Y. K. The effect of oxidative debris on the laser desorption/ionization efficiency of graphene oxide derivatives for mass spectrometric analysis of small molecules and synthetic polymers. *Anal. Sci.* **2019**, *35*, 1097−1102.

(21) Luo, G.; Chen, Y.; Daniels, H.; Dubrow, R.; Vertes, A. Internal energy transfer in laser desorption/ionization from silicon nanowires. *J. Phys. Chem. B* **2006**, *110*, 13381−13386.

(22) Lai, S. K. M.; Cheng, Y. H.; Tang, H. W.; Ng, K. M. Silver-gold alloy nanoparticles as tunable substrates for systematic control of ion-desorption efficiency and heat transfer in surface-assisted laser desorption/ionization. *Phys. Chem. Chem. Phys.* **2017**, *19*, 20795.

(23) Kim, Y. -K.; Na, H.-K.; Kwack, S.-J.; Ryoo, S-R.; Lee, Y.; Hong, S.; Hong, S.; Jeong, Y.; Min, D.-H. Synergistic effect of graphene oxide/MWCNT films in laser desorption/ionization mass spectrometry of small molecules and tissue imaging. *ACS Nano* **2011**, *5*, 4550−4561.

(24) Dagan, S.; Hua, Y.; Boday, D. J.; Somogyi, A.; Wysocki, R. J.; Wysocki, V. H. Internal energy deposition with silicon nanoparticle-

assisted laser desorption/ionization (SPALDI) mass spectrometry. *Int. J. Mass Spectrom.* **2009**, *283*, 200−205.